

AD-A165 722


NRL Memorandum Report 5741


Estimating the Scattering Coefficient of the Ocean Surface for High-Frequency Over-the-Horizon Radar

R. O. PILON AND J. M. HEADRICK

*Radar Techniques Branch
Radar Division*

March 28, 1986



DTIC
ELECTE
MAR 27 1986


NAVAL RESEARCH LABORATORY
Washington, D.C.

Approved for public release; distribution unlimited.

86 3 27 002

DTIC FILE COPY

DISCLAIMER NOTICE

**THIS DOCUMENT IS BEST QUALITY
PRACTICABLE. THE COPY FURNISHED
TO DTIC CONTAINED A SIGNIFICANT
NUMBER OF PAGES WHICH DO NOT
REPRODUCE LEGIBLY.**

SECURITY CLASSIFICATION OF THIS PAGE

AD-A165722

REPORT DOCUMENTATION PAGE

1a. REPORT SECURITY CLASSIFICATION UNCLASSIFIED			1b. RESTRICTIVE MARKINGS		
2a. SECURITY CLASSIFICATION AUTHORITY			3. DISTRIBUTION/AVAILABILITY OF REPORT Approved for public release; distribution unlimited.		
2b. DECLASSIFICATION/DOWNGRADING SCHEDULE			5. MONITORING ORGANIZATION REPORT NUMBER(S)		
4. PERFORMING ORGANIZATION REPORT NUMBER(S) NRL Memorandum Report 5741			7a. NAME OF MONITORING ORGANIZATION		
6a. NAME OF PERFORMING ORGANIZATION Naval Research Laboratory		6b. OFFICE SYMBOL (if applicable) Code 5320		7b. ADDRESS (City, State, and ZIP Code)	
6c. ADDRESS (City, State, and ZIP Code) Washington, DC 20375-5000			9. PROCUREMENT INSTRUMENT IDENTIFICATION NUMBER		
8a. NAME OF FUNDING/SPONSORING ORGANIZATION Space & Naval Warfare Sys. Com.		8b. OFFICE SYMBOL (if applicable) Code 6243		10. SOURCE OF FUNDING NUMBERS	
8c. ADDRESS (City, State, and ZIP Code) Washington, DC 20360-5100		PROGRAM ELEMENT NO. 64725N		PROJECT NO. X1779	WORK UNIT ACCESSION NO. DN291-215
11. TITLE (Include Security Classification) Estimating the Scattering Coefficient of the Ocean Surface for High-Frequency Over-the-Horizon Radar					
12. PERSONAL AUTHOR(S) Pilon, R. O. and Headrick, J. M.					
13a. TYPE OF REPORT Interim		13b. TIME COVERED FROM TO		14. DATE OF REPORT (Year, Month, Day) 1986 March 28	
				15. PAGE COUNT 23	
16. SUPPLEMENTARY NOTATION					
17. COSATI CODES			18. SUBJECT TERMS (Continue on reverse if necessary and identify by block number)		
FIELD	GROUP	SUB-GROUP	Radar, Over-the-horizon, Ocean surface, High-frequency, Scattering coefficient, Sea clutter		
			(Continues)		
19. ABSTRACT (Continue on reverse if necessary and identify by block number) Several methods for determining the radar scattering coefficient of the ocean surface, σ^0 , all based on the technique developed by Trizna, have been applied to two sets of High-Frequency Over-the-Horizon data. One specific method is found to yield the best results. A method of operation of an HF OTH system to allow the estimation of σ^0 is recommended.					
20. DISTRIBUTION/AVAILABILITY OF ABSTRACT <input checked="" type="checkbox"/> UNCLASSIFIED/UNLIMITED <input type="checkbox"/> SAME AS RPT. <input type="checkbox"/> DTIC USERS			21. ABSTRACT SECURITY CLASSIFICATION UNCLASSIFIED		
22a. NAME OF RESPONSIBLE INDIVIDUAL R. O. Pilon			22b. TELEPHONE (Include Area Code) (202) 767-4873		22c. OFFICE SYMBOL Code 5320

DD FORM 1473, 84 MAR

83 APR edition may be used until exhausted.
All other editions are obsolete

SECURITY CLASSIFICATION OF THIS PAGE

18. SUBJECT TERMS (Continued)

Cross-section
Remote sensing
Oblique sounder

CONTENTS

INTRODUCTION	1
THE BASIC TECHNIQUE	1
SOME POSSIBLE METHODS FOR ESTIMATING σ^0	4
REVIEW OF RESULTS	17
CONCLUSIONS	18
OPERATIONS DESIGN CONSIDERATIONS	18
REFERENCES	18

Distribution For	
Mr. CRA&I	<input checked="" type="checkbox"/>
Mr. TIB	<input type="checkbox"/>
Mr. [unclear]	<input type="checkbox"/>
J. [unclear]	
By _____	
Date _____	
Approved _____	
Special Agent/CR	
Dist	Special
A-1	23

ESTIMATING THE SCATTERING COEFFICIENT OF THE OCEAN SURFACE FOR HIGH-FREQUENCY OVER-THE-HORIZON RADAR

INTRODUCTION

The radar scattering coefficient of the ocean surface, σ^0 , is a basic quantity in radar remote sensing of the ocean surface for such purposes as sea state estimation, weather and storm tracking, the estimation of the propagation properties of the atmosphere and the quantitative aspects of the detection and monitoring of targets on and above the ocean surface. One of the most important uses of σ^0 is in the real-time assessment of a surveillance radar's performance capabilities. If σ^0 is known, the ratio of the backscatter from the ocean surface to noise can be used to indicate the radar's performance indices P_D (probability of detection) and P_{FA} (probability of false alarm). Also, an estimation of σ^0 can aid in the determination of the cross-section of a target detected by an High-Frequency Over-the-Horizon (HF OTH) radar system. The cross-section of the target is computed using σ^0 , the area of the radar footprint on the ocean surface and the ratio of the power level of the target to that of the sea clutter in the doppler spectrum.

In HF OTH radar systems the propagation path losses in terms of amplitude and polarization rotation are not fully known. Thus, it is very difficult to estimate σ^0 directly from the radar equation. The technique developed by Trizna [1] is based on the doppler characteristics of the first and second order radar scatter from the wind disturbed ocean surface, allowing an estimation of σ^0 from internal doppler spectrum power ratios. It was developed through extensive averaging of ground wave data obtained using relatively long coherent integration times (CIT).

The operational efficiency of an HF OTH system used for surveillance does not, however, allow the option of extensive averaging in time. The purpose of the present investigation is to extend the technique to OTH skywave propagation and apply it to relatively short CIT data and shorter averaging times. The basic technique is reviewed in the next Section. This is followed by a discussion of some of the possible methods of applying the procedure to two sets of HF OTH radar data collected on 13 August 1981. The results of the various methods are reviewed and it is concluded that one specific method yields the best results. A method of operation is recommended for actual data collection.

THE BASIC TECHNIQUE

The technique developed by Trizna is based on data collected using vertically polarized antennas and ground wave propagation. It is directly applicable to OTH skywave propagation in yielding a scattering coefficient identical to that which would be measured using vertically polarized antennas and ground wave propagation, i.e. σ_{VV}^0 . However, a 3 dB modification must be introduced in determining the cross-section of a target.

The effective scattering coefficient for an OTH radar is smaller than σ_{vv}^o . During propagation through the ionosphere radio waves experience polarization rotation (Faraday rotation). The effect is such that the polarization of the radar energy incident on the ocean surface undergoes several rotations (progressing mainly in range) within the resolution cell of a single beam. Since the scattering coefficient for horizontal polarization (at HF frequencies and near grazing incidence) is very small compared to that for vertical polarization, the effective scattering coefficient for a radar resolution cell illuminated via skywave propagation is 3 dB smaller than σ_{vv}^o .

The usual target is, however, of small spatial extent relative to the spatial period of the rotating polarization of the incident radar energy. At any given instant of time the cross-section of the target is not being spatially averaged in the same manner as that of the ocean surface. Therefore, Trizna's technique for determining the cross-section of a target on the ocean surface may be applied directly to OTH radar data if EITHER 3 dB is subtracted from σ_{vv}^o OR the detected power level of the sea clutter return is increased by 3 dB in comparing it with that of the target. In determining the cross-section of a target above the ocean surface, multipath effects must also be considered.

The pattern of rotating polarization incident of the ocean surface and targets within the resolution cell also moves over the surface with time. The polarization of the radar energy incident on a target at any given instant of time or during a given CIT is unknown. Therefore, the cross-section of a target computed using the data for a given CIT is an average cross-section for the unknown range of polarization vector orientations incident on the target during the CIT. Normally, time averaging over a period of one or significantly more cycles of polarization rotation is required to obtain a reasonable estimate of the targets cross-section. Thus, such cross-section determinations are an average over all polarizations. By virtue of its motion, an aircraft would probably pass through many more cycles of polarization rotation than a ship on station.

It should be noted that the values given for the various estimates for σ^o in this report ARE NOT EFFECTIVE SCATTERING COEFFICIENTS unless otherwise stated. They are instead estimates of σ_{vv}^o .

An example of an HF OTH radar doppler spectrum obtained for a CIT of 51.2 seconds is shown in Fig. 1. The two first order Bragg peaks and the second order return appear near zero Hz doppler frequency. The return at +1.1 Hz is from a ship. The estimation of σ^o relies on the measures rho, the power ratio of the two first order Bragg peaks, and zeta, the power ratio of the stronger first order Bragg peak to the second order power level midway between the two first order Bragg peaks. The radar cross-section of the ship may then be computed using σ^o , the area of the ocean surface illuminated by the radar beam and the power ratio mu of the target to the total sea clutter. In this instance the power level of the total sea clutter return may be approximated by that of the stronger first order Bragg peak.

The radar scattering coefficient of the ocean surface is determined using the nomograph shown in Fig. 2 and the equation [1]

$$\sigma^o = -38.9 + \Delta + (\rho/2) + 10 \log [1 + 10^{-\rho/10}] ,$$

where σ^o , Δ and ρ are expressed in decibels. In Fig. 1 $\rho = 20.2$ dB and $\zeta = 26.8$ dB. Using the measure rho, the nomograph indicates that the acute angle theta between the azimuthal direction of propagation of the radar energy and the major axis of the ocean wave spectrum was 38 degrees. The $\Delta = 0$ dB reference line for a CIT of 51.2 seconds is 0.1 dB below that shown for CIT = 50 seconds and $\alpha = 0.0081$ (Phillips' constant). The value for Δ to be used in the above equation is seen to be +2.4 dB. Therefore, $\sigma^o = -26.4$ dB(sqm/sqm).

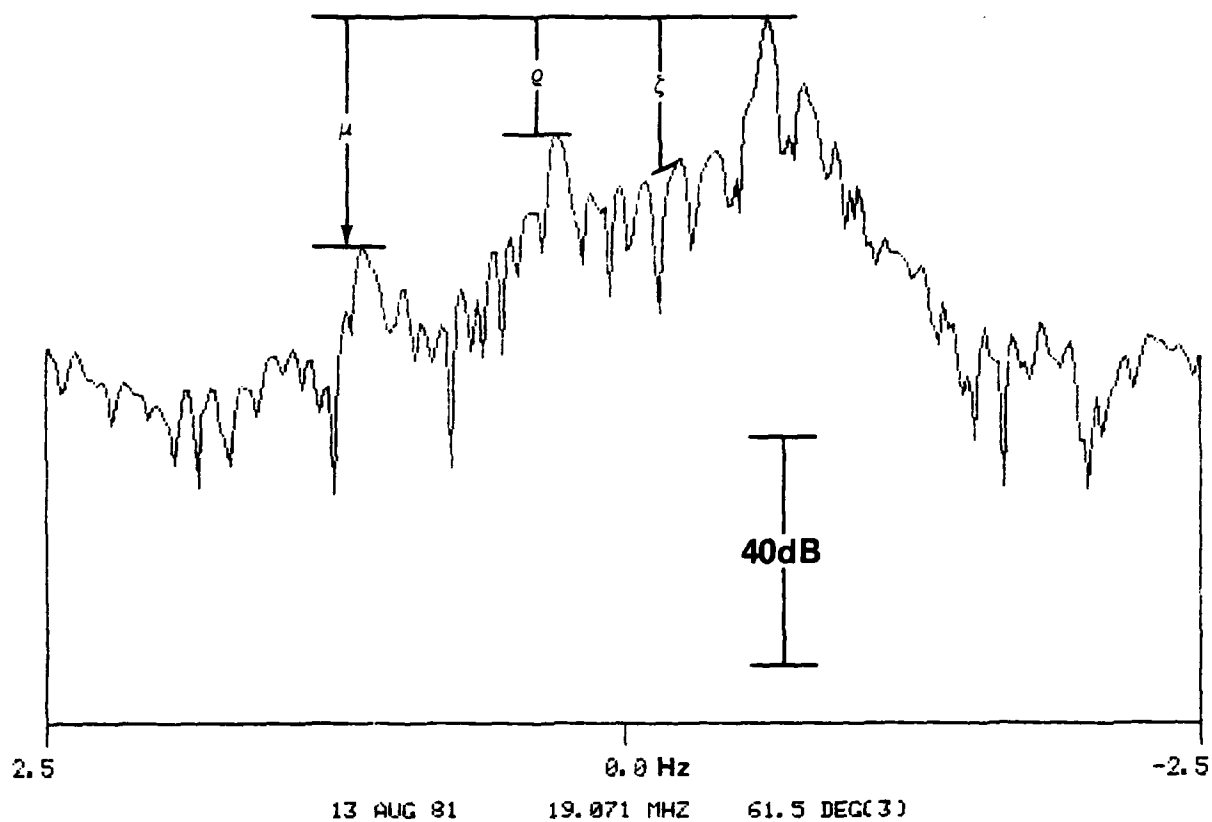


Fig. 1. An example of HF OTH radar data displaying the received power as a function of doppler frequency.

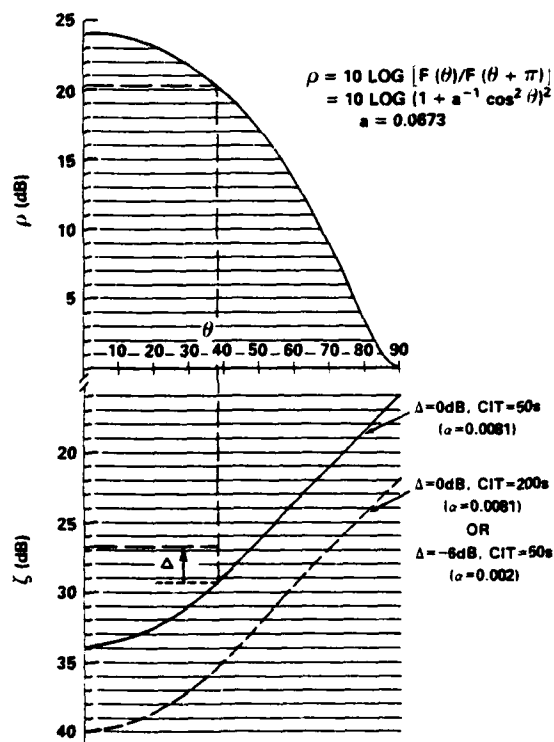


Fig. 2. The nomograph used in determining σ^0 (adapted from ref. [1]).

The effective scattering coefficient of the resolution cell was then $\sigma^0 - 3.0 = -29.4$ dB(sqm/sqm). Since its area was 90.6 dB(sqm), the effective cross-section of the surface within the resolution cell was 61.2 dB(sqm). The cross-section of the target relative to the effective cross-section of the sea clutter was the measure μ (-40.3 dB), yielding a cross-section for the ship of 20.9 dB(sqm). This value for the cross-section of the ship is for the unknown range of polarization vector orientations incident on the ship during the 51.2 second CIT. Based on the computations reviewed in the next Section, the radar scattering coefficient of the ocean surface, the effective cross-section of the surface and the cross-section of the ship indicated by the data from this particular CIT are too large by about 5 dB. This is an example of one of the extremes encountered in the data.

For data analysis purposes, equations have been used in place of the nomograph. The ocean wave spectral spreading function assumed by Trizna determined the upper curve. Its functional form is given in Fig. 2. The lower empirical curve has been approximated for this study. The error in the computed value for Δ ($\alpha = 0.0081$) with respect to the nomograph is less than ± 0.4 dB for $0^\circ \leq \theta \leq 45^\circ$ and $+0.0, -0.1$ dB for $45^\circ \leq \theta \leq 90^\circ$.

This basic technique for estimating σ^0 is dependent on the ocean wave spectrum of the water wavelengths being sensed by the radar [2]. Oceanographic knowledge of the ocean wave spectrum is, however, incomplete. The areas in which the incompleteness of oceanographic knowledge affects the determination of σ^0 are the azimuthal shape of the spectrum as a function of water wavelength, and hence radar wavelength, and the shape of the spectrum with fetch and with time, as discussed below.

If a steady wind has been blowing over a period of several hours, and over a long expanse (a few hundreds of miles), or fetch, of ocean surface toward the area being measured, the azimuthal spreading factor or shape of the spectrum for water wavelengths of about 10 m and shorter is approximately cosine squared, as assumed here. The quantitative manner in which the spreading factor differs from cosine squared for longer water wavelengths and shorter fetches and times is not completely known.

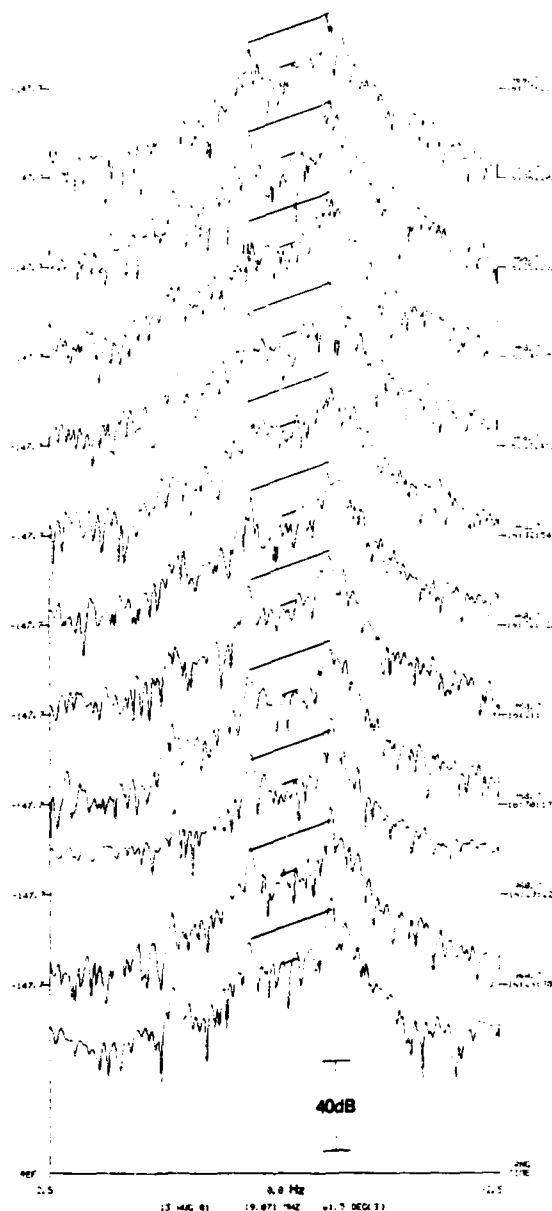
For areas of the ocean surface towards which the wind has been blowing steadily for at least 3 to 6 hours, and over a fetch of at least 150 nautical miles, the estimated error in σ^0 , when sensed at radar frequencies greater than 15 MHz, is ± 3 dB. Water wavelengths of 10 m and shorter respond fairly rapidly to surface winds, and thus this region of the ocean spectrum can be assumed to be in equilibrium for the above conditions. For radar frequencies of 5 to 15 MHz the estimated error is ± 6 dB, and ± 10 dB for frequencies of 1 to 5 MHz. These errors increase as the angle between the direction of the wind and the direction of propagation of the radar energy approaches 90° , i.e. as θ approaches 0 dB.

This method is assumed to be valid, but with increased error, for shorter periods of a steady wind after near calm conditions and for a short period after the weather system starts to decay. This method is not, however, applicable to areas experiencing changing meteorological conditions. Therefore, the applicability of this method of determining σ^0 can be enhanced through the use of surface meteorology forecasts and hindcasts.

SOME POSSIBLE METHODS FOR ESTIMATING σ^0

It should be noted that σ^0 , with or without identifying subscripts, should be read as σ_{vv}^0 with or without the same identifying subscripts.

Fig. 3. A falling raster display of the received power as a function of doppler frequency for successive coherent integration times (CIT = 51.2 s) in the interval 16:28:30 to 16:38:02 GMT on 13 August 1981.



The falling raster display shown in Fig. 3 is a plot of the received power as a function of doppler frequency for successive coherent integration times. All of the returns are from the same range, as indicated by the range in nautical miles along the right edge of the Figure, just above the time (GMT) for each CIT. The termini of the lines connecting the center frequencies of the two first order Bragg peaks indicate the relative powers of the two peaks based on the median power levels of similar data. The vertical separation between the lines is a constant 25 dB - the power offset in the falling raster display. The center points of the short lines through the second order Bragg return, midway between the two first order peaks, also indicate the relative power levels of similar data. The purpose of these lines is to represent reference power levels against which CIT to CIT variations in power may be visualized. It is seen that the power levels of interest in determining ρ and ζ vary both in absolute and relative magnitude.

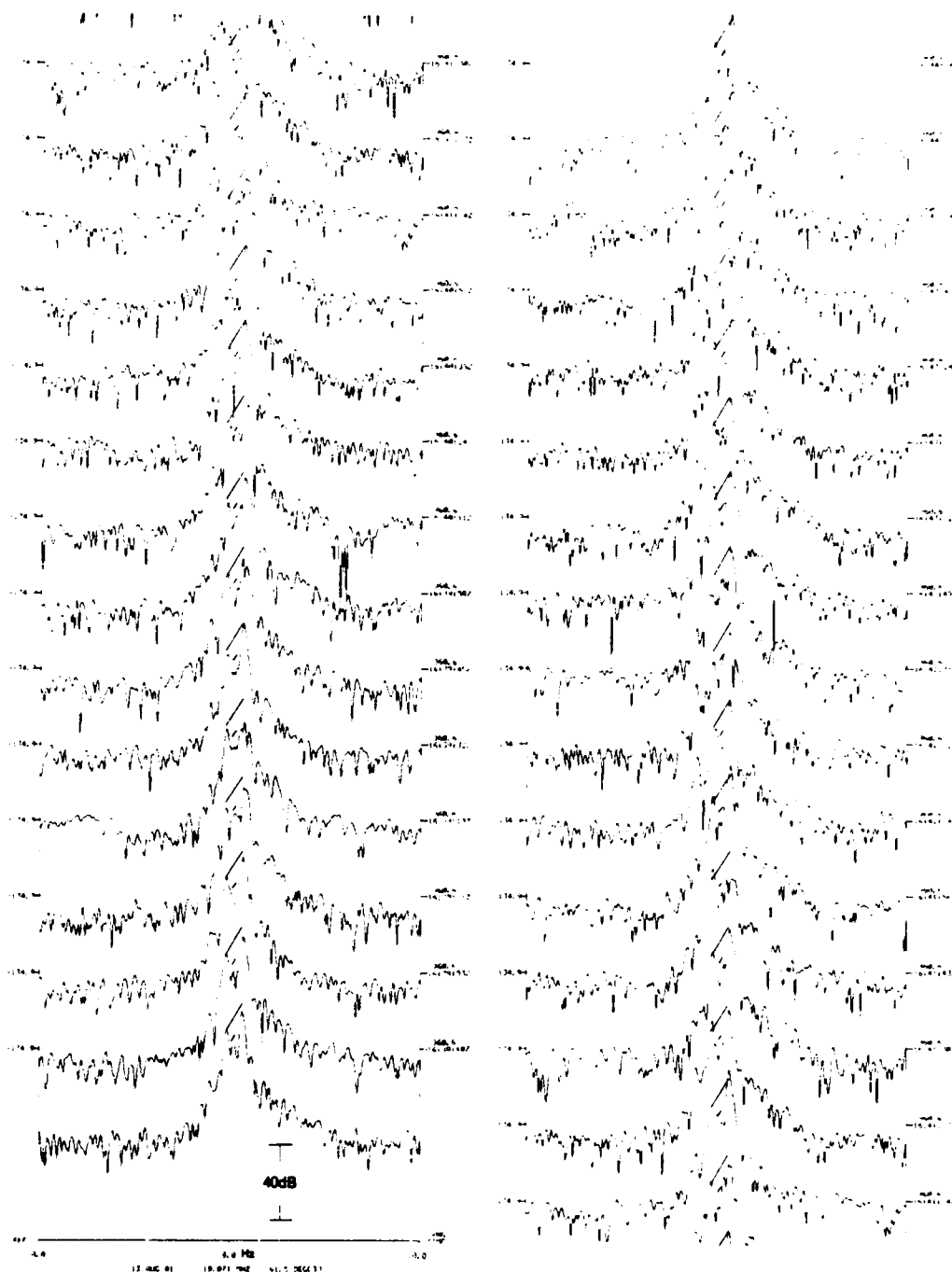


Fig. 4. A falling raster display of the received power as a function of doppler frequency for successive coherent integration times (CIT = 12.8 s) in the interval 16:38:40 to 16:44:33 GMT on 13 August 1981.

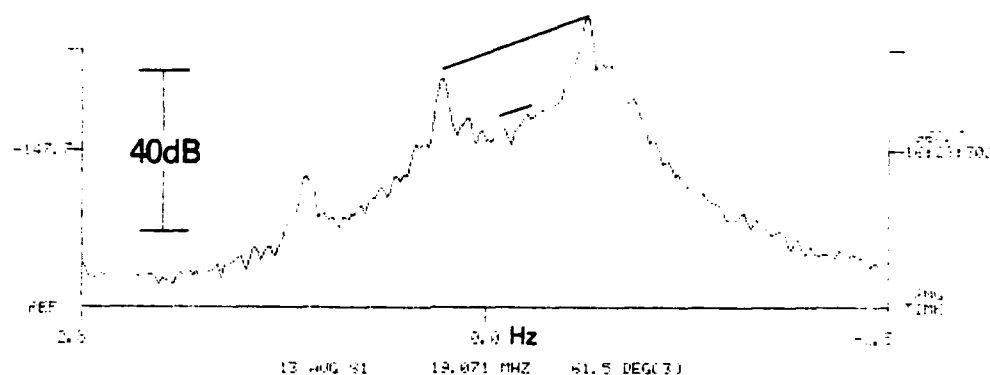


Fig. 5. The average power, at each doppler frequency, for the eleven traces shown in Fig. 3.

The data shown in Fig. 3 were obtained with a CIT of 51.2 seconds. Data obtained immediately after that displayed in Fig. 3, but with a CIT of 12.8 seconds, are similarly displayed in Fig. 4. These data, as well as other data sets, also indicate that the power levels of interest in determining rho and zeta vary erratically from CIT to CIT.

Fig. 5 displays the average power (the square of the average of the square root of the power levels) at each doppler frequency for the eleven traces shown in Fig. 3. The reference power levels are the same as those shown in Fig. 3. The values of rho and zeta measured from the average power levels are 15.5 and 25.2 dB, yielding a σ^0 of -31.2 dB(sq m/sq m). Averages of the first, second and third sets of nine traces from the 27 shown in Fig. 4, and the average of all 27, are similarly displayed in Figs. 6, 7, 8 and 9. The values of rho and zeta measured from the average power levels yield values for σ^0 of -35.6, -38.4, -33.2 and -35.5 dB(sq m/sq m). Thus, the average power levels for these data sets also exhibit significant disparities in the value for σ^0 .

In computing the cross-section of a moving target, either a ship or an aircraft, the scattering coefficient would be determined for the range bins which follow the track of the target. The return from a ship is apparent in Figs. 3 and 4 at a doppler frequency of approximately +1.1 Hz. The ship was tracked through both time periods based on its maximum power return. Of the eleven coherent integration times in the interval from 1628 to 1638 hours (Fig. 3), the ship was determined to be in range bin 28 (968.7 nautical miles) seven times and in range bin 27 (960.6 nmi) a total of four times, as it slowly approached the radar. Of the 27 coherent integration times in the interval from 1638 to 1645 hours (Fig. 4), the ship appeared in range bin 27 a total of 15 times, with a small number of extreme excursions from range bins 24 (936.3 nmi) to 30 (993.0 nmi).

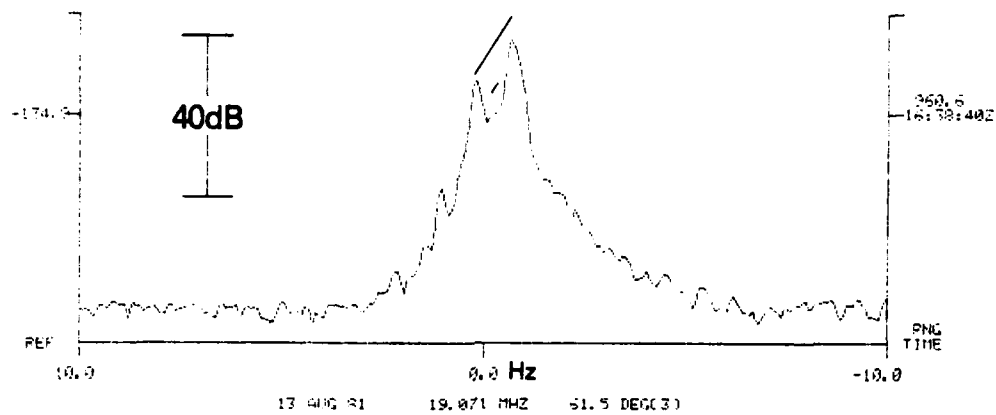


Fig. 6. The average power, at each doppler frequency, for the first set of nine traces shown in Fig. 4.

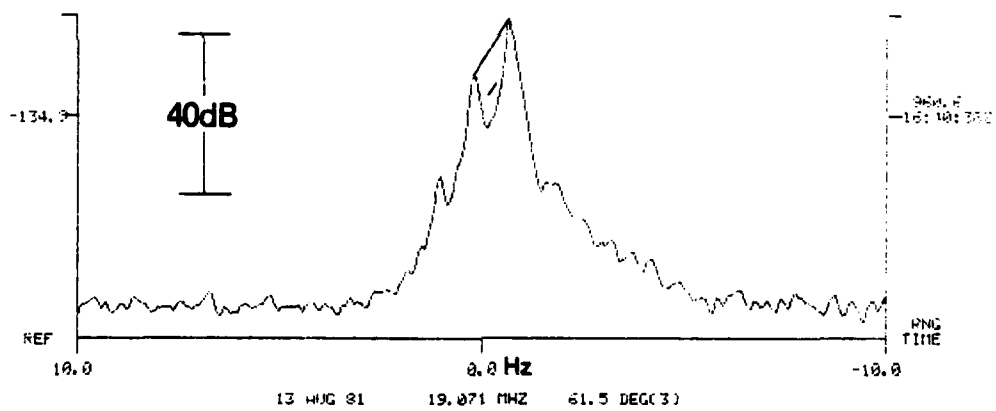


Fig. 7. The average power, at each doppler frequency, for the second set of nine traces shown in Fig. 4.

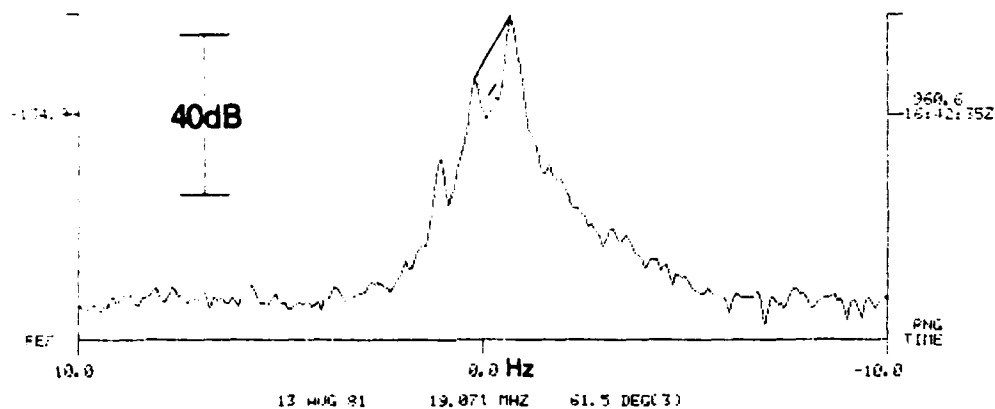


Fig. 8. The average power, at each doppler frequency, for the third set of nine traces shown in Fig. 4.

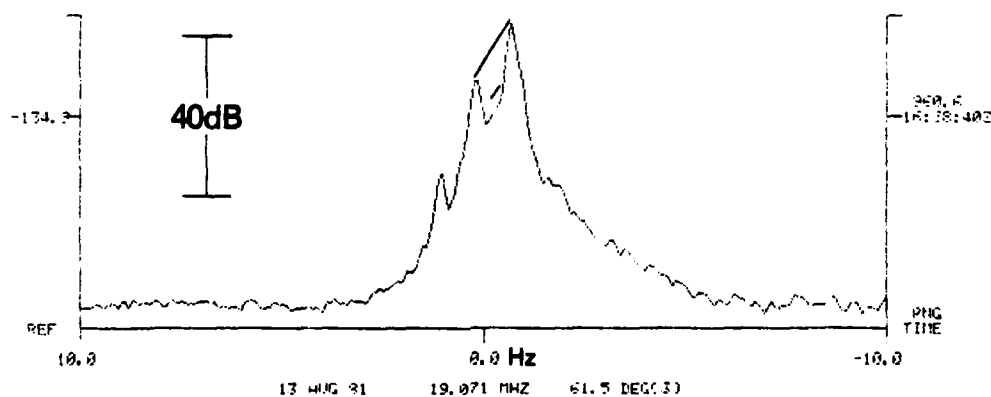
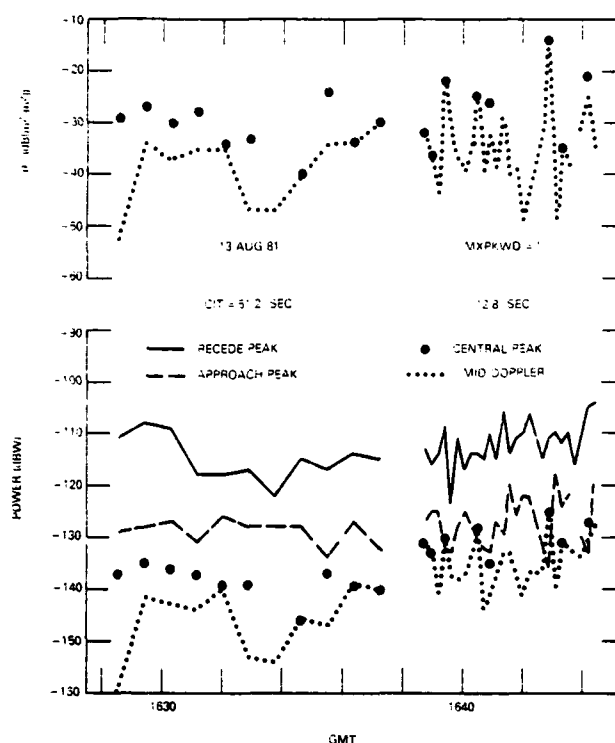


Fig. 9. The average power, at each doppler frequency, for all 27 traces shown in Fig. 4.

Fig. 10. The variation in the received power levels (using the peak width criteria $MXPKWD=1$) for successive coherent integration times, and the resulting values for σ^0 computed for each CIT.



The data obtained from tracking the ship have been processed in three different ways. The results are displayed in the lower halves of Figs. 10, 11 and 12. In Fig. 10, $MXPKWD$, the maximum peak width input for the tracking programs, is unity. Thus, the power levels plotted for the recede and approach peaks and the central peak are the maximum power levels attained in a single, discrete doppler frequency bin. The recede peak is the first order Bragg peak due to waves propagating away from the radar and the approach peak is that due to waves propagating towards the radar. A central peak is a peak appearing within the central 20% (or 5 doppler bins, whichever is greater) of the doppler interval between the two first order Bragg peaks. For the 51.2 second data, in which the separation of the two first order Bragg peaks ranged from 45 to 47 doppler bins (0.0195 Hz per bin), the central region is the middle 9 doppler bins (0.176 Hz). The average separation for the 12.8 second data was nearly 11.6 doppler bins (0.0781 Hz per bin). For such data the central 20% would be too small an interval to search for a second order peak. Thus, the central region was defined to be the middle 5 doppler bins (0.391 Hz). A central peak cannot always be found. One is missing in the data from 1628 to 1638 hours and only eight were found in the data for 1638 to 1645 hours. The mid doppler power level is that in the doppler bin midway between the doppler bins of the two first order Bragg peaks.

In Fig. 11, $MXPKWD$ is three. Thus, the power levels were obtained by integrating the square root of the powers in the doppler bin of maximum power (the mid doppler bin in the case of mid doppler) and one doppler bin on each side of it. The integrated amplitudes were then squared to yield the appropriate power levels. In Fig. 12, where $MXPKWD$ is 19, the integration is over the doppler bin of maximum power return ± 9 bins or the full width of the peak, whichever is less. The full width of a peak is taken to be the doppler width between the points at which the powers increase to form adjacent peaks. The doppler interval resulting from integrating over the mid doppler bin ± 9 bins would be too broad. Therefore, that data is not included in Fig. 12. The erratic fluctuations in the power levels evident in Figs. 3 and 4 are also evident in the lower halves of Figs. 10, 11 and 12.

Fig. 11. The variation in the received power levels (using the peak width criteria MXPKWD=3) for successive coherent integration times, and the resulting values for σ^0 computed for each CIT.

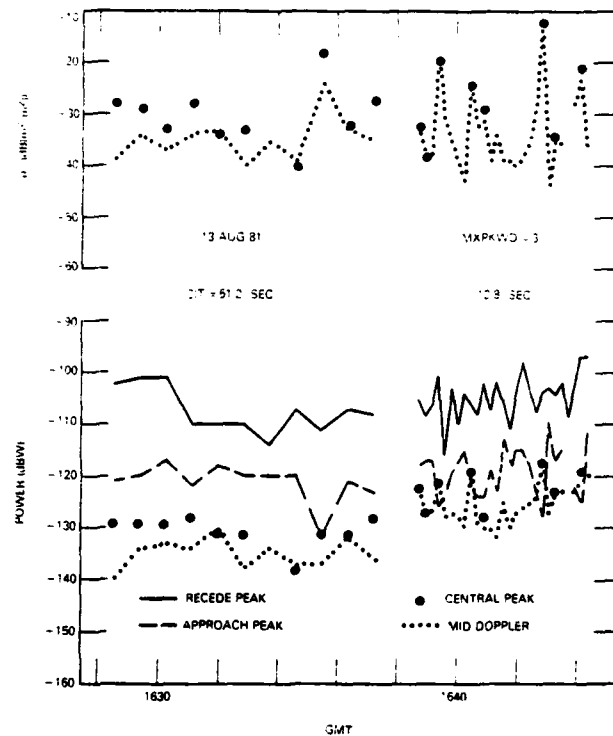
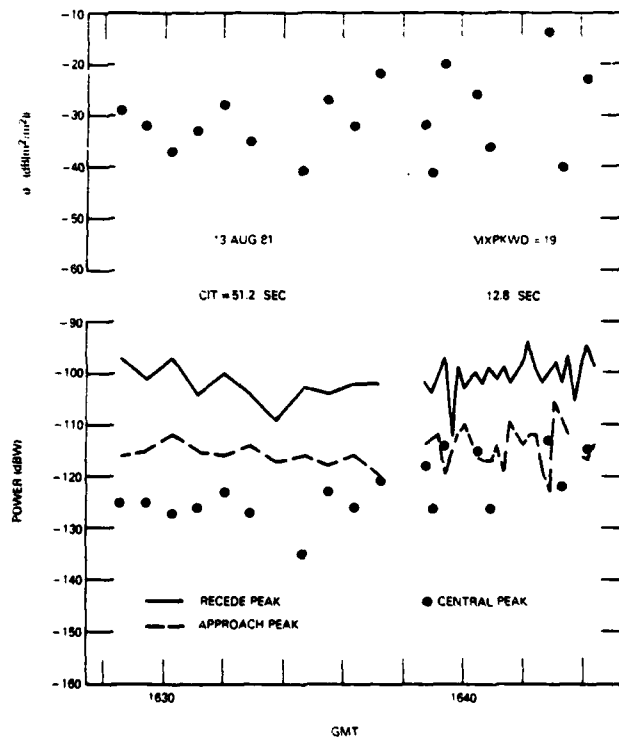


Fig. 12. The variation in the received power levels (using the peak width criteria MXPKWD=19) for successive coherent integration times, and the resulting values for σ^0 computed for each CIT.



These three different ways of measuring the power in a peak are being investigated in an effort to determine the measure that will yield the best practical results. The first measure, MXPWD = 1, is the simplest to implement. However, if the power in the mid doppler bin is used to determine zeta, that power level may be at the peak of a central peak, in the trough between two near-central peaks or at some power level between these two. Thus, zeta may be too large, leading to a low estimate for σ° . The use of MXPWD = 3 or slightly larger may alleviate this problem. A maximum peak width of 19 has been used for tracking targets. A cursory examination of some of the available data indicated that the full peak width of most of the targets was about eleven doppler bins. Nineteen was chosen to accommodate some peak broadening. The full width of a central peak is usually much less than 19 doppler bins. The two first order peaks are, however, much wider. This disparity may also lead to a high value for zeta and a low estimate for σ° .

An estimation of σ° requires a determination or estimation of the measures rho and zeta. While it can be seen from Figs. 3, 4, 10, 11 and 12 that the value for rho fluctuates erratically, the measurement itself is straightforward. However, the near continuum of the second order scatter midway between the two first order Bragg peaks that is available when using relative long coherent integration times and extensive averaging, is not evident in the data displayed here. Thus, what second order power level should be used to determine zeta?

Three different second order power levels will be investigated. They are the power level of a central peak, the power level in the doppler bin midway between the two first order Bragg peaks, and a power level based on the measure rho and the assumption of ocean wave spectral saturation ($\Delta = 0$) at the appropriate water wavelengths.

The various ways in which σ° may be estimated from these power levels are indicated in Fig. 13, as applied to a sample of the data extracted from Fig. 11. The estimates σ_A° and σ_C° are based on the power levels of the central peaks. The estimate σ_A° is determined by first computing a σ_n° from the recede, approach and central peak power levels for each CIT. A mean and median σ_A° are then computed from the σ_n° values. Alternatively, σ_C° is determined by first computing the mean and median of the dB power levels for the recede, approach and central peaks in the data set, and then computing σ_C° (mean and median). The estimates σ_B° and σ_D° are determined in a similar manner, using the mid doppler power levels in place of the central peak power levels. The estimates σ_E° and σ_F° are based on the recede and approach peak power levels and the assumption of ocean wave spectral saturation. The estimate σ_E° is determined by first computing a σ_n° using the measure ρ_n and $\Delta = 0$ for each CIT. A mean and median σ_E° are then computed from the σ_n° values. Alternatively, σ_F° is determined by first computing the mean and median of the dB power levels for the recede and approach peaks in the data set and then computing ρ and σ_F° (mean and median) assuming $\Delta = 0$. These six methods of estimating σ° will be discussed below.

$$\sigma_A^\circ$$

The values of σ_n° computed from the data available in each CIT are displayed in the upper halves of Figs. 10, 11 and 12. The values based on the central peaks are indicated by the blackened circles. The mean, standard deviation and median of the values for each time period, identified by the coherent integration time and MXPWD, are tabulated in TABLE 1. There are too few data points in most of these data sets to allow a meaningful computation of the standard deviation. These values will only be utilized for a rough comparison of the spread in values of σ_A° and σ_E° with those of σ_E° .

The experimental values for σ° may be compared against a theoretical value for σ° based on a cosine squared spreading function for the ocean spectrum and a total spectral energy content in agreement with the work of Barrick [3], as in ref. [1]. It will be assumed that the ocean spectrum

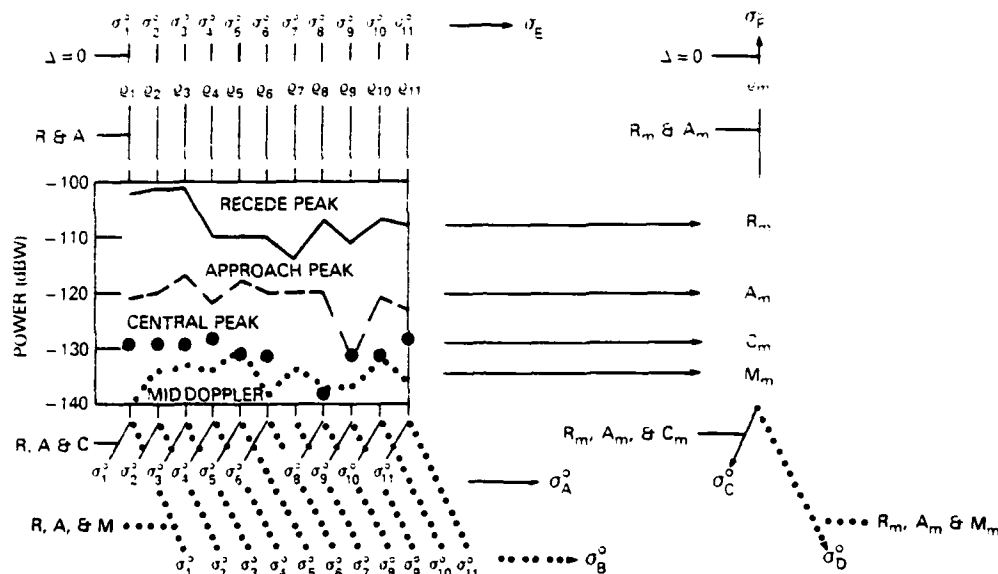


Fig. 13. A sample of the data extracted from Fig. 11 and some of the various ways in which an estimate of σ^0 may be determined using the recede peak (R), approach peak (A), central peak (C) or mid doppler (M) power levels for each CIT, or R_m , A_m , C_m or M_m , the mean (or median) of the dB power levels for the data set.

at the water wavelengths scattering the 19.071 MHz radar energy, i.e. 7.9 meters for the two first order Bragg peaks and 5.6 meters for the second order return at mid doppler, was saturated. The mean of the dB values of rho for all 111 pairs of first order Bragg peaks plotted in Figs. 10, 11 and 12 is 14.3 dB, and the median is 14 dB. This implies an angle theta of 58° and a theoretical value for σ^0 of -31.6 dB(sq m/sq m). This value is less than ten of the twelve values for σ_A^0 , lending credence to the assumption of spectral saturation at 7.9 and 5.6 meter water wavelengths.

While the values of σ_A^0 for a CIT of 51.2 seconds is in good agreement with the theoretical value, the values for 12.8 seconds are mostly several dB too high.

$$\sigma_B^0$$

The values of σ_n^0 based on the mid doppler power levels are joined by dotted lines in the upper halves of Figs. 10 and 11. The mean, standard deviation and median values of σ_B^0 are also tabulated in TABLE 1. It is seen that these values are consistently lower than those based on the central peaks. The standard deviations are, however, comparable.

$$\sigma_C^0$$

Values for σ^0 may also be computed from the mean and median of the dB power levels for each of the six sets of data displayed in the lower halves of Figs. 10, 11 and 12. The values computed from the recede, approach and central peak power levels are tabulated in TABLE 1 under the σ_C^0 heading. It is seen that these values are comparable to those for σ_A^0 for a CIT of 51.2 seconds and that the values for a CIT of 12.8 seconds are now comparable to those for 51.2 seconds and the theoretical value of -31.6 dB(sq m/sq m).

$$\sigma_D^0$$

The values for σ^0 computed from the mean and median of the dB power levels of the recede and approach peaks and mid doppler are tabulated in TABLE 1 under the heading σ_D^0 . Like those for σ_B^0 , these values are consistently lower than those based on the power levels of the central peaks.

$$\sigma_E^0$$

The theoretical value for σ^0 of -31.6 dB(sq m/sq m) was computed assuming that the ocean spectrum at water wavelengths of 7.9 and 5.6 meters was saturated. This is a reasonable assumption at these wavelengths and the experimental values computed thus far indicate that the assumption was valid for these sets of data. If the same assumption is made in computing σ_A^0 for each CIT, only rho has to be determined. The values of rho for the data displayed in Figs. 10, 11 and 12 are displayed in Fig. 14. The corresponding values of σ_E^0 ($\Delta = 0$) are shown along the right edge of the Figure for the theoretically valid interval $0 \text{ dB} \leq \rho \leq 24 \text{ dB}$. As indicated above, the mean of all 111 values for rho is 14.3 dB and the median is 14 dB. These two measures yield an average value for σ^0 of -31.6 dB(sq m/sq m). The mean, standard deviation and median values for σ^0 computed directly from the values of rho ($\Delta = 0$) for each individual data set are tabulated under the heading σ_E^0 in TABLE 1. The mean and median values are of course very close to the average value of -31.6 dB(sq m/sq m).

The standard deviation of the values are mainly one-half to one-third of those tabulated for σ_A^0 . This indicates that in computing σ^0 for each CIT using rho and zeta, one-third to one-half of the spread in the value of σ_A^0 is due to the variability in the measurement of rho and one-half to two-thirds of the spread is due to the variability in the measurement of zeta. This also holds for a comparison of the standard deviations for σ_E^0 and σ_B^0 .

$$\sigma_F^0$$

The assumption of ocean spectrum saturation at 7.9 and 5.6 meter water wavelengths may also be applied to the mean and median of the dB power levels for each data set. The results are tabulated under the heading σ_F^0 in TABLE 1. These values are in good agreement with the theoretical value for σ^0 of -31.6 dB(sq m/sq m).

The assumption of spectral saturation yields a "maximum" value for σ^0 . If σ^0 is computed in the manner of either σ_E^0 or σ_F^0 , the actual value of σ^0 would be lower by the amount that the ocean spectrum is below saturation at the water wavelengths responsible for the first and second order scattering of the radar energy.

The estimates σ_C^0 , σ_D^0 and σ_F^0 have been computed from the mean and median of the dB power levels for ensembles of coherent integration times. These mean and median levels may be obtained from probability plots, such as those shown in Fig. 15. These computer generated plots are labeled in units of the standard deviation sigma. The total plot error is less than ± 1 division except in the six columns along each side of the plot, where the error increases rapidly.

The recede and approach power levels are identified by "R" and "A", central peaks by "Z" and mid doppler power levels by "M". The power return from the ship is identified by "T" and the "+" and "-" symbols represent the noise power levels in the extreme positive and negative doppler bins.

TABLE 1

CIT (s)	MXPKWD (doppler bins)	σ_A^0 (dB)			σ_B^0 (dB)			σ_C^0 (dB)		σ_D^0 (dB)		σ_E^0 (dB)			σ_F^0 (dB)	
		mean	std. dev.	median	mean	std. dev.	median	mean	median	mean	median	mean	std. dev.	median	mean	median
51.2	1	-31.7	3.8	-30	-39.5	6.4	-35	-31.4	-32	-39.6	-39	-31.6	1.9	-32.2	-31.7	-32.2
51.2	3	-31.6	3.9	-30.5	-35.9	2.5	-35	-30.9	-31	-35.4	-35	-31.7	2.0	-31.7	-31.8	-32.4
51.2	19	-32.7	4.3	-32	—	—	—	-31.4	-31	—	—	-31.8	1.5	-31.7	-31.8	-31.7
12.8	1	-28.3	5.9	-25.5	-35.7	6.5	-35	-30.4	-31	-35.4	-35	-31.0	2.6	-31.0	-31.0	-30.8
12.8	3	-28.4	6.5	-27	-34.3	5.9	-32.5	-31.0	-31	-34.4	-36	-31.4	2.5	-31.7	-31.6	-31.7
12.8	19	-31.1	7.7	-29	—	—	—	-32.1	-30	—	—	-31.7	2.2	-31.7	-31.8	-31.7

σ_A^0 : Computed using the recede peak, approach peak and central peak power level for each CIT.

σ_B^0 : Computed using the recede peak, approach peak and mid doppler power level for each CIT.

σ_C^0 : Computed using the mean (median) of the dB power levels for the recede peaks, approach peaks and central peaks in each data set.

σ_D^0 : Computed using the mean (median) of the dB power levels for the recede peaks, approach peaks and mid doppler frequency in each data set.

σ_E^0 : Computed using the recede and approach peak power levels for each CIT ($\Delta=0$).

σ_F^0 : Computed using the mean (median) of the dB power levels for the recede and approach peaks in each data set ($\Delta=0$).

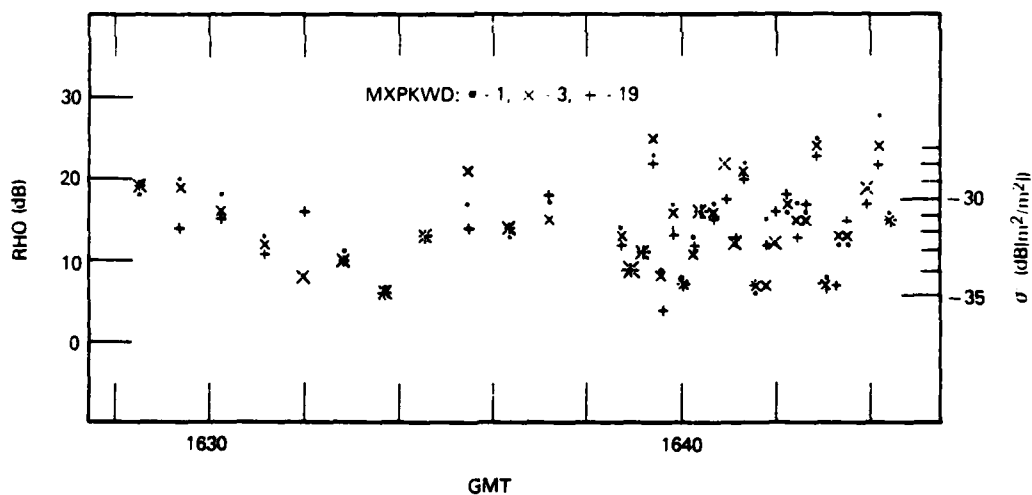


Fig. 14. The values of rho for all of the data displayed in Figs. 10, 11 and 12 (where MXPKWD = 1, 3 and 19) and the corresponding values for σ^0 , assuming spectral saturation at water wavelengths of 7.9 and 5.6 meters (i.e. $\Delta = 0$).

The data for each power level are seen to approximate straight lines, indicating a Gaussian distribution. The median may be taken as the power level at $\sigma = 0$ or the average of the two or three power levels nearest $\sigma = 0$. A straight line may also be fitted to the data between σ equals -1 and +1, -2 and +2 or some other limits. The mean power level would then be taken where the straight line intersects $\sigma = 0$.

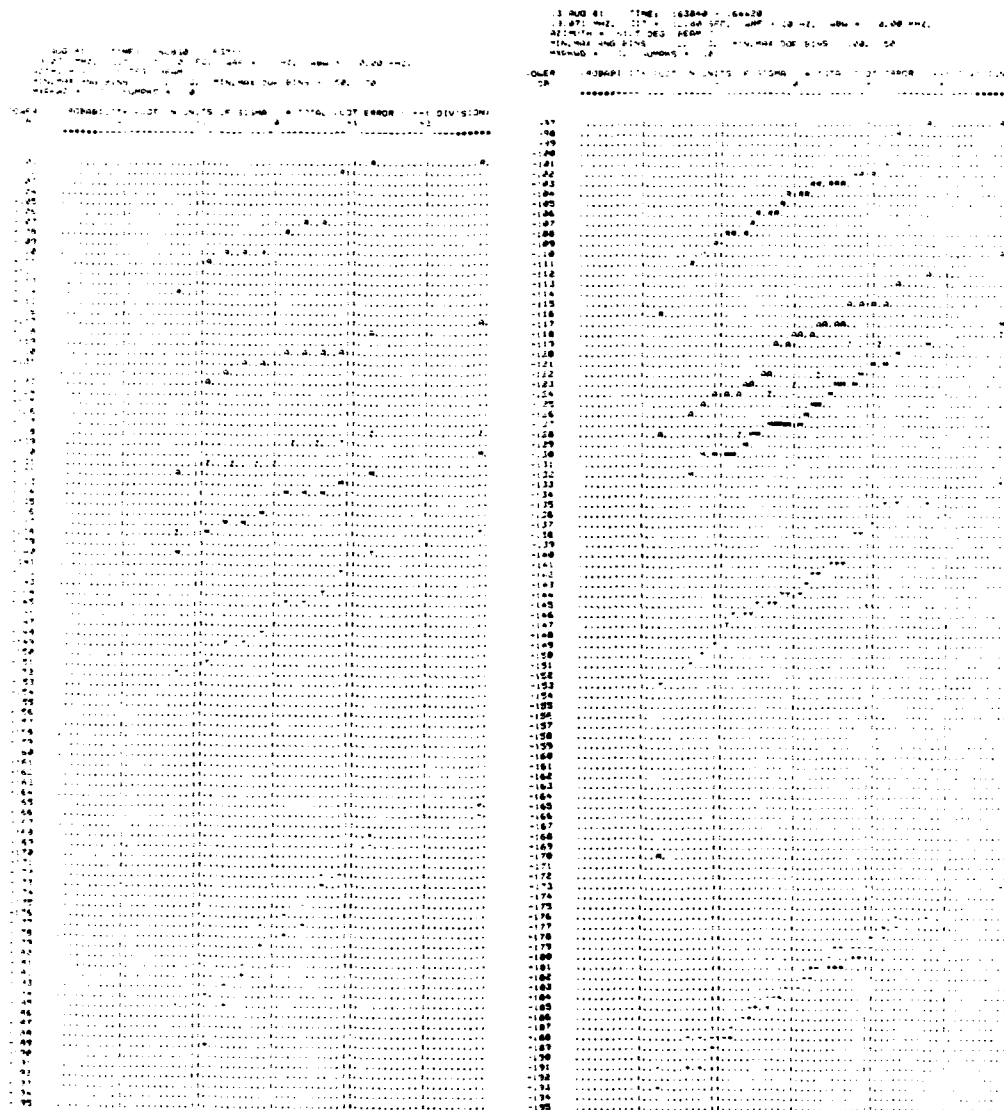


Fig. 15. Probability plots, in units of the standard deviation σ , of the power levels (MXPKWD=3) for the recede (R), approach (A), central peak (Z), mid doppler (M) and ship (T) returns and the noise power levels (MXPKWD=1) in the extreme positive (+) and negative doppler bins.

REVIEW OF RESULTS

The various methods for estimating σ° that have been discussed in the previous Section have been applied to a very small data set. The major conclusions that may be drawn, however, are consistent with the methodology and probably applicable in general.

The most self-consistent values for σ° have been obtained when only the two first order Bragg peaks are considered (σ_E° and σ_F°). These peaks represent the two strongest returns in the radar data. This fact, together with the reasonable assumption of saturation of the ocean wave spectrum at the wavelengths responsible for the radar return, lend credence to either of these two methods for estimating σ° . The spread in the values for σ_E° (mean) and σ_F° (mean) is 0.8 dB, while the spread is 1.2 dB for σ_E° (median) and 1.6 dB for σ_F° (median). The smaller spread in the mean values with respect to the median values is also apparent in the other methods for estimating σ° .

The assumption of saturation of the ocean wave spectrum, although reasonable in some instances, is not generally valid. Therefore, the method yielding σ_C° may yield more reliable results when used on a continuous basis or as a spot check on spectral saturation.

The method yielding σ_C° makes use of the two strong first order Bragg peaks and the central peak, when it is evident. This method yields the second most consistent values for σ° , values that are, in general, less than 1 dB larger than those for σ_E° and σ_F° . The spreads in the values for σ_C° , 1.7 dB for the mean and 2 dB for the median, are greater than those found for σ_E° and σ_F° .

The main problem with this method is that a central peak is not always evident. One central peak (9%) was missing in the 51.2 second CIT data and 19 (70%) were not evident in the 12.8 second CIT data. Thus, a combination of the method yielding σ_C° with that for either σ_E° or σ_F° may produce the best results, especially for short coherent integration times.

None of the three methods reviewed above exhibit a consistent variation with MXPKWD, the number of doppler bins over which the energy in the peak is integrated.

The method yielding σ_A° is similar to that for σ_E° except that the power of the central peak is used in the determination of σ_n° for each CIT. It is also similar to that for σ_F° except that σ_n° is determined for each CIT and then the mean and median values for σ_n° are computed, instead of computing σ° from the mean and median of the dB power levels. The spreads in the values for σ_A° are 4.3 dB for the mean and 6.5 dB for the median. These overall spreads, and those within each subset, are greater than those encountered above. The greater spreads are due to the influence of the individual central peak power levels. While the values for a CIT of 51.2 seconds are comparable to those for σ_C° , σ_E° and σ_F° , five of the six values for a CIT of 12.8 seconds are several dB larger.

The values for σ_B° and σ_D° are consistently smaller than the others, by as much as 6.8 dB. This is due to the use of mid doppler power levels rather than central peak power levels. The mid doppler power level may be at the peak of a central peak, in the trough between two adjacent peaks or at some power level between these two. Thus, zeta is too large and σ° is too small.

CONCLUSIONS

It may be concluded from the preceding Section that the best estimate of σ^0 is obtained using the mean values of the two first order Bragg peaks and a central peak. Thus, the coherent integration time must be long enough to permit the detection and measurement of the power in a central peak.

The criteria for the presence of a peak in this work is that the power level two doppler bins on one side of the assumed peak must be less than or equal to the power level of the peak and that the power level two doppler bins on the other side of the assumed peak must be less than that of the peak. This formal procedure for the establishment of a central peak may be relaxed in establishing the two first order Bragg peaks. The large amplitude of these two peaks relative to all others and their approximate location and separation in doppler frequency indicate that these two peaks may be established by searching for the maximum power levels at the appropriate doppler frequencies.

The results displayed for σ_c^0 , σ_e^0 and σ_f^0 in Table 1 do not exhibit any consistent variation with the degree of integration of the energy in the peaks. Therefore the data processing may be simplified by considering only the peak power levels (MXPWD = 1).

OPERATIONS DESIGN CONSIDERATIONS

The best estimates of σ^0 are obtained for coherent integration times of about 30 seconds and longer. This is due to the fact that the variance of the measured power levels decrease with time and that a central power level becomes easier to establish. This conflicts, however, with the short coherent integration time, or dwell time, required when a large area of the ocean surface is to be monitored in a timely manner. Such dwell times would be on the order of one second.

An integral part of a short dwell time surveillance radar is an oblique sounder for frequency management and performance capability assessment. The sounder is used to obtain ionospheric and other propagation information that is not available from short dwell time target search data. Since the revisit time constraints of the oblique sounder are not critical, it is recommended that it also be used in a radar mode, with a dwell time of 30 seconds or longer, to produce a map of σ^0 over the area under surveillance. Such a map could be used directly with the short dwell time search data to establish the cross-section of detected targets.

REFERENCES

1. D.B. Trizna, "Estimation of the Sea Surface Radar Cross Section at HF from Second-Order Doppler Spectrum Characteristics," NRL Report 8579, May 1982. AD A115230
2. D.B. Trizna, Naval Research Laboratory, Washington, D.C., private communication, Sept. 1985.
3. D.E. Barrick, "First-Order Theory and Analysis of MF/HF/VHF Scatter from the Sea," IEEE Trans. AP, AP-20, pp. 2-10, 1972.